

# Enhancement of amplification characteristics in a plasma-filled Cherenkov laser at millimeter wavelengths

T. Thumvongskul,<sup>a)</sup> A. Hirata,<sup>b)</sup> G. Zaginaylov,<sup>c)</sup> and T. Shiozawa

*Department of Communication Engineering, Osaka University, Suita, Osaka 565-0871, Japan*

(Received 27 July 1999; accepted for publication 9 November 1999)

On the basis of the fluid model of the electron beam, amplification characteristics of a two-dimensional plasma-filled Cherenkov laser at 100 GHz bands are analyzed. By injecting a dense plasma into the background of a Cherenkov laser, the coupling between a relativistic electron beam and an electromagnetic wave at millimeter wavelengths has been improved, and the weak beam-wave interaction problem has become less serious. In particular, we show that due to electron-ion collisions in the background plasma, proper choices of parameters are essential for good operation in this regime. The numerical results indicate that a Cherenkov laser with background plasma can generate higher output power with a greatly enhanced growth rate at a more reasonable interaction length. The plasma injection, in addition, enables the device to gain more output power with a higher beam current. © 2000 American Institute of Physics. [S0021-8979(00)05604-8]

## I. INTRODUCTION

As a good candidate for coherent high-power and tunable sources at short millimeter and submillimeter wavelengths, the Cherenkov free-electron laser has been extensively studied experimentally<sup>1–3</sup> and theoretically.<sup>4–8</sup> It has a promising future in various applications, such as space communications, high-resolution radars, remote sensing, etc.<sup>9</sup> In a typical vacuum Cherenkov device, however, the electromagnetic (EM) field, which interacts with a relativistic electron beam, concentrates around the dielectric surface of a waveguide and decays exponentially in the transverse direction, leading to a weak beam-wave interaction. This becomes more significant at higher frequencies, since the field decays more rapidly from the dielectric surface. In such a situation, an attempt to inject an electron beam into the region of high field intensity near the dielectric surface can cause more difficulties regarding dielectric breakdown and the control of beam transport. Moreover, increasing the beam thickness in a weak field would not help enhance the beam-wave interaction,<sup>7</sup> but result in essentially low efficiency devices.

The injection of a dense plasma into the background of the Cherenkov laser modifies the beam-wave interaction, and the performance of the device is greatly enhanced.<sup>10–13</sup> Specifically, we can either: (i) inject an electron beam into the device at a distance far enough from the dielectric surface, or (ii) even use a thicker beam to interact with a less nonuniformly distributed electric field, and yet obtain a more effective beam-wave coupling. Filling the device with a dense plasma allows the system to generate more EM output power with a significantly enhanced growth rate. Moreover,

the background plasma plays an important role in neutralizing the space-charge force in the electron beam, and facilitating the beam transport. Since the plasma lightens the repulsive force which causes the beam to broaden and increases the space-charge limited current of the electron beam,<sup>14</sup> it is easier to achieve a higher output power with a higher beam current. In addition, when a dense plasma occupies the entire area above the dielectric sheet, a relative field strength at the dielectric surface is lowered, which relaxes the problem of electric charges accumulating there.

Recently, there have been several demonstrations on relativistic electron beam devices with background plasma around 10 GHz.<sup>10,13</sup> However, the weak beam-wave interaction and other problems stated above become more significant at millimeter wavelengths. Thus, in this paper, we investigate the amplification characteristics of the Cherenkov device at 100 GHz bands. In order to generate millimeter wave radiation, the stationary background plasma with densities of  $10^{12}$ – $10^{15}$  cm<sup>-3</sup>, which is about 2–3 orders larger than those used at 10 GHz bands, is required. However, with such a dense plasma, the effect of electron-ion collisions cannot be ignored. Note that the use of a plasma column with such high density and a length of more than 2 m has been reported in some experiments in related fields (see Ref. 15 for example).

The organization of this paper is as follows. In Sec. II, we show the dispersion relation for the coupled EM and space-charge waves in a two-dimensional (2-D) plasma-filled Cherenkov laser. The plasma modes, choices for the operating point, and the maximum growth rate are also discussed in this section, as well as the effect of electron-ion collisions in the background plasma. With the aid of numerical simulation based upon the fluid model of the electron beam, we discuss the growth and saturation characteristics of the EM wave in Sec. III, taking into account the decrease in the drift velocity of the electron beam. From our numerical analysis, we find that an enhanced EM power can be extracted at a more reasonable interaction length, at the expense of a little fraction

<sup>a)</sup> Author to whom correspondence should be addressed; electronic mail: tipyada@comm.eng.osaka-u.ac.jp

<sup>b)</sup> Research Fellow of the Japan Society for the Promotion of Science for Young Scientists.

<sup>c)</sup> On leave of absence from Kharkov State University, Kharkov, 310-077, Ukraine.

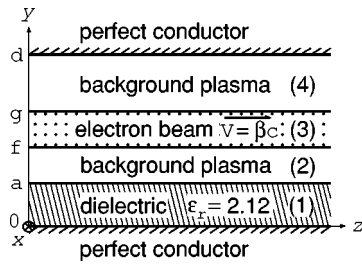


FIG. 1. Geometry of the problem.

of the beam energy lost to the kinetic energy in the background plasma. A brief conclusion and remark are given in Sec. IV.

## II. DISPERSION RELATION AND SPATIAL GROWTH RATE FOR COUPLED WAVES

A 2-D parallel-plate model of a plasma-filled Cherenkov laser illustrated in Fig. 1 is considered. A dense background plasma with homogeneous density profile occupies the entire region over the dielectric sheet with relative permittivity  $\epsilon_r$  and thickness  $a$  through the upper conductor plate located at the distance  $d-a$  above the dielectric sheet. At the distance  $f-a$  from the dielectric surface, a planar relativistic electron beam with initial velocity  $V_0$  and thickness  $g-f$  is injected. For simplicity, we assume that both the background plasma and the electron beam are restricted to move only along the  $z$  direction by a sufficiently large axial magnetic field. We also ignore the collision that may occur between the background plasma and the dielectric.

### A. Wave equations and dispersion relation

Solving first the relativistic equation of motion separately for the background plasma and the electron beam, with the aid of the continuity equation, we find the corresponding current densities. Substituting them into Maxwell's equations, we obtain the wave equation for the TM mode in each region specified in Fig. 1 as

$$\begin{aligned} \left( \frac{\partial^2}{\partial y^2} + p_y^2 \right) \tilde{E}_z &= 0 \text{ in region (1)} \\ \left( \frac{\partial^2}{\partial y^2} + k_{y1}^2 \right) \tilde{E}_z &= 0 \text{ in regions (2) and (4),} \end{aligned} \quad (1)$$

$$\left( \frac{\partial^2}{\partial y^2} + k_{y2}^2 \right) \tilde{E}_z = 0 \text{ in region (3)}$$

where

$$p_y^2 = \epsilon_r \frac{\omega^2}{c^2} - k_z^2, \quad h_y^2 = k_z^2 - \frac{\omega^2}{c^2},$$

$$k_{y1}^2 = -\epsilon_p h_y^2, \quad k_{y2}^2 = -\epsilon_{pb} h_y^2,$$

$$\epsilon_p = 1 - \left( \frac{\omega_p}{\omega} \right)^2, \quad (2)$$

$$\epsilon_{pb} = 1 - \left( \frac{\omega_p}{\omega} \right)^2 - \left\{ \frac{\omega_b}{\gamma(\omega - k_z V)} \right\}^2,$$

$$\omega_p^2 = \frac{e^2 N_{p0}}{\epsilon_0 m_0}, \quad \omega_b^2 = \frac{e^2 N_{b0}}{\gamma \epsilon_0 m_0},$$

$$\gamma = \frac{1}{\sqrt{1 - \beta^2}}, \quad \beta = \frac{V}{c}.$$

Here,  $\tilde{E}_z$  is the Fourier amplitude for the axial electric field. The symbols  $\omega$ ,  $c$ ,  $\epsilon_0$ ,  $m_0$  and  $e$  denote, respectively, the operating frequency, the velocity of light in vacuum, the permittivity of vacuum, and the rest mass and electric charge of the electron. The plasma frequencies of the background plasma and the electron beam  $\omega_p$  and  $\omega_b$  correspond to their number densities  $N_{p0}$  and  $N_{b0}$ , respectively. In the absence of the background plasma,  $\omega_p = 0$ , and in the absence of the electron beam,  $\omega_b = 0$ . In addition,  $k_z$  is the longitudinal wave number, while  $p_y$ ,  $h_y$ ,  $k_{y1}$ , and  $k_{y2}$  are, respectively, the transverse wave numbers in the dielectric, vacuum, background plasma and beam regions. The other field components  $\tilde{E}_y$  and  $\tilde{B}_x$  can be derived from the expressions for  $\tilde{E}_z$  obtained from the wave equations (1) in each region. By imposing the proper boundary conditions at each interface on the field components,<sup>11,16</sup> we obtain the following dispersion relation for the TM waves:

$$\begin{aligned} D(\omega, k_z) = & \frac{\epsilon_r h_y}{p_y \sqrt{\epsilon_p}} \cdot \{ \tan k_{y1}(f-a) + \tan k_{y1}(d-g) \} + \tan p_y a \cdot \left\{ \tan k_{y1}(d-g) \cdot \tan k_{y1}(f-a) + \frac{\sqrt{\epsilon_p}}{\sqrt{\epsilon_{pb}}} \tan k_{y1}(f-a) \right. \\ & \cdot \tan k_{y2}(g-f) + \frac{\sqrt{\epsilon_{pb}}}{\sqrt{\epsilon_p}} \tan k_{y2}(g-f) \cdot \tan k_{y1}(d-g) - 1 \left. \right\} - \left\{ \frac{\epsilon_{pb}}{\epsilon_p} \tan k_{y1}(f-a) \cdot \tan k_{y1}(d-g) - 1 \right\} \\ & \cdot \frac{\epsilon_r h_y}{p_y \sqrt{\epsilon_{pb}}} \tan k_{y2}(g-f) = 0. \end{aligned} \quad (3)$$

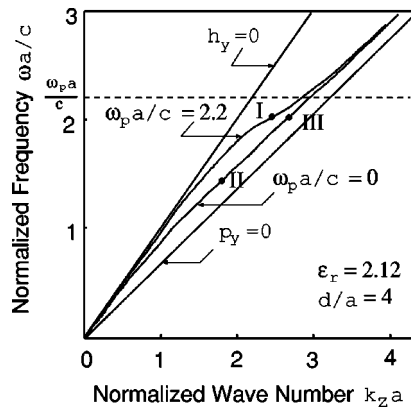


FIG. 2. Dispersion relation in the absence of the electron beam ( $\omega_p a/c = 0, 2.2$ ). Only the lowest-order mode is shown.

Relation (3) reveals coupling between the negative-energy space-charge wave propagated along the relativistic electron beam and the slow EM wave propagated along the dielectric waveguide. In the absence of the electron beam, we show in Fig. 2 the dispersion curves for the cases where the waveguide is filled and not filled with plasma. Due to the presence of the background plasma (i.e.,  $\omega_p \neq 0$ ), the modified dispersion curve is upshifted to higher frequencies, depending on the value of  $\omega_p$ . On the dispersion diagram, the operating point of the coupled system can be approximately obtained at the intersection of the dispersion curve for the case without the beam shown in Fig. 2 and the beam line approximated by  $\omega = k_z V_0$ . Then, it is obvious from the dispersion diagram that the system with background plasma (i) can operate at higher frequencies when the beam with an appropriate value of drift velocity is injected, or (ii) can be driven by a higher beam current at the same operating frequency, leading to a higher output power.

## B. Plasma modes

Besides the modification of EM wave branches, the background plasma also results in an appearance of some additional plasma modes near the asymptotic line ( $p_y = 0$ ), when the background plasma owns a rather large density.<sup>12</sup> A relativistic electron beam with a certain value of beam velocity can couple with both the modified upshifted EM mode and the plasma modes. The synchronous frequency for the fundamental plasma wave (which is expected to have the largest spatial growth rate among the plasma modes) is much lower than that for the modified EM wave. This may introduce undesired lower frequency components which consume a fraction of energy in the coupling process. However, the maximum growth rate for the plasma waves for the values of our parameters is much lower than that for the modified EM wave.

## C. Field distribution and choice for the operating point

For the coupling between the modified EM and space-charge waves, which is of interest to us, the dispersion relation (3) has two complex roots for  $k_z$  in a particular range of

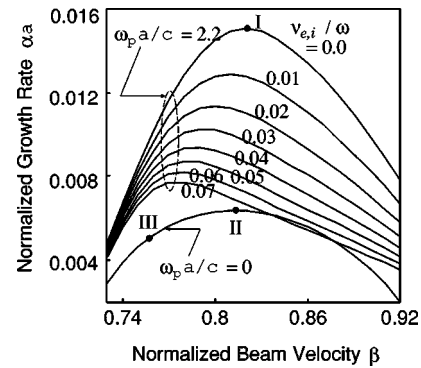


FIG. 3. Spatial growth rate versus normalized beam velocity  $\beta$  [ $\omega_p a/c = 0, 2.2$  and  $(g-f)/a = 0.533$ ]. Spatial growth rates at I, II and III correspond to the three points in Fig. 2. Values of the ratio between electron-ion collision frequency and operating frequency  $v_{e,i}/\omega$  are indicated on the curves for the plasma-filled case.

frequencies. The two roots are complex conjugate to each other, corresponding to growing and decaying waves. The decaying wave does not significantly take part in the interaction process, since it vanishes within a few wavelengths. Thus, for a given value of frequency, we find the longitudinal wave number and the spatial growth rate (i.e., the real and imaginary parts of  $k_z$ , respectively) for a growing wave of a particular TM mode, by numerically solving the dispersion relation (3).

When  $\omega < \omega_p$ , the axial electric field in the plasma region does not exponentially decay in the transverse direction, and can flatly distribute if the values of parameters are appropriately specified. At the operating frequency  $\omega$ , we determine the value of  $\omega_p$  satisfying the condition  $\omega < \omega_p$  (point I in Fig. 2), in order to gain an EM field with relatively large magnitude, which can effectively interact with the electron beam. At the same time, we obtain an EM field with a nearly uniform distribution about the beam position. This can allow only a small variation of axial electric field over the beam cross section, leading to a more stable interaction. At the regime where  $\omega > \omega_p$ , the field in the plasma region behaves as a transversely evanescent wave, hence decaying exponentially similar to the field in vacuum. However, the decay rate is much smaller than that for the vacuum device, even though the frequency is higher. The spatial growth rate for the system with plasma is apparently enhanced (see Fig. 3), due to a modified field distribution that provides a substantial field magnitude of the axial field interacting with the electron beam. To compare with the plasma-filled case (point I), we select the operating points II and III in Fig. 2 for the vacuum case, which correspond to the values of the spatial growth rate denoted by the points with the same notation in Fig. 3. For a given value of  $\omega_p$ , points I and II provide the maximum values of the spatial growth rate for the plasma-filled and vacuum cases (see Sec. IID), respectively, at slightly different values of the beam drift velocity. Point III is also chosen to compare with point I in terms of the coupling and growth characteristics at the same operating frequency. Note that by appropriately specifying the dimensions of the model in Fig. 1 (specifically, the value of dielec-

tric thickness  $a$ ), operating frequencies at the three points fall in the millimeter wave region.

At a distance apart from the dielectric surface, the field strength in the plasma device is yet strong enough to interact effectively with the beam. Thus we can inject the beam at a distance far enough from the dielectric surface. This also suggests possibilities to increase the cross section of the interaction space in order to improve the heat transfer condition and relax the requirements on the beam transport.<sup>12</sup> Further, it is possible to use the beam with larger thickness in order to gain a more effective coupling and higher output power. Furthermore, in our model for which we assume that the background plasma occupies the whole area above the dielectric sheet, the intensity of electric field at the dielectric surface is lowered. This enables the problem of electric charges accumulating there to be less serious.

#### D. Maximum growth rate

From Fig. 3, we notice that there exists a maximum spatial growth rate for the coupled waves. In general, the value of the spatial growth rate is proportional to  $\{\partial D(\omega, k_z)/\partial k_z\}^{-1/3}$ ,<sup>11</sup> i.e., inversely proportional to the slope of the dispersion curve  $\partial\omega/\partial k_z$  or the group velocity  $v_g$ . This agrees well with the physical argument that, when the EM wave carries an energy more slowly (for a small value of  $v_g$ ), it gains a larger amount of energy from the electron beam (at the same field strength in place of the beam). Thus at the minimum of  $\partial\omega/\partial k_z$ , we obtain the peak value of the spatial growth rate at points I and II in Fig. 3 for the plasma and vacuum devices, respectively. Also, it should be pointed out that the peak value of the spatial growth rate becomes larger and sharper as the background plasma density increases. We expect that it achieves the absolute maximum at the plasma density which provides a rough equality of synchronous frequencies for the upshifted EM and plasma waves. (See an example of the growth rate as a function of the background plasma density  $\omega_p$  in Ref. 11.) In this case, an excitation of a hybrid mode synchronizing with the electron beam (with strong beam-wave coupling) is possible.<sup>12</sup>

#### E. Electron-ion collisions in the background plasma

Because of the very high density of the background plasma at the operation regime considered here, we could not possibly ignore the collision between electrons and ions in the plasma. We take into account the effect from this kind of collision via the collision frequency  $\nu_{e,i}$  term. By replacing  $\varepsilon_p$  and  $\varepsilon_{pb}$  described in Eq. (2) by<sup>17</sup>

$$\begin{aligned}\varepsilon_p &= 1 - \frac{\omega_p^2}{\omega(\omega - j\nu_{e,i})}, \\ \varepsilon_{pb} &= 1 - \frac{\omega_p^2}{\omega(\omega - j\nu_{e,i})} - \left\{ \frac{\omega_b}{\gamma(\omega - k_z V)} \right\}^2,\end{aligned}\quad (4)$$

where  $j$  is the unit imaginary number, we can yet numerically calculate the spatial growth rate from the dispersion relation, Eq. (3). As obviously seen from Fig. 4, when the collision between electrons and ions in the background plasma becomes violent (for large values of  $\nu_{e,i}$ ), the coupled waves

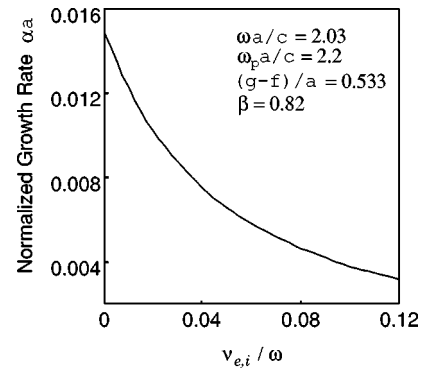


FIG. 4. Spatial growth rate vs electron-ion collision frequency  $\nu_{e,i}/\omega$ .

own a poor spatial growth rate which, at certain circumstances, can probably be no longer superior to that in the vacuum device. However, we can estimate the value of  $\nu_{e,i}$  for our model in the 100 GHz region by<sup>17</sup>

$$\nu_{e,i} = \frac{5.5N}{T^{3/2}} \ln \left( \frac{220T}{N^{1/3}} \right), \quad (5)$$

where  $T$  and  $N$  denote the temperature (K) and the plasma density ( $\text{cm}^{-3}$ ), respectively. Equation (5) gives the value of the collision frequency for a fully ionized unmagnetized plasma, which may be somewhat different from that for a fully magnetized plasma, but is sufficient for the estimation in our analysis. (A strong magnetic field contributes only in the expression under logarithm in Eq. (5).<sup>17</sup>) For the background plasma with  $T \sim 1000$  K and  $N \sim 10^{14} \text{ cm}^{-3}$ , the ratio  $\nu_{e,i}/\omega$  is on the order of  $10^{-2}$ . The spatial growth rate versus the normalized beam velocity for various values of  $\nu_{e,i}/\omega$  plotted in Fig. 3 reminds us that a selection of appropriate parameters is critical for gaining a better spatial growth rate. However, with suitable values of parameters, we can yet insist that the spatial growth rate in the plasma device is enhanced beyond that for the vacuum device. In addition, we also notice from Fig. 3 that, when the electron-ion collisions in the background plasma are taken into account, the peak value of the spatial growth rate shifts to a region where the beam drift velocity is smaller, depending on the collision frequency.

#### III. GROWTH AND SATURATION CHARACTERISTICS

In a Cherenkov laser with background plasma, the plasma kinetic energy grows in proportion to the EM wave energy. The growths of both energies are compensated for by the growth of the space-charge wave with negative energy, which is equivalent to the decrease in the kinetic energy of the electron beam. The ratio of the kinetic energy gained by the background plasma  $\bar{W}_{\text{plasma}}$  to the EM wave energy  $\bar{W}_{\text{EM}}$  can be found from

$$\frac{\bar{W}_{\text{plasma}}}{\bar{W}_{\text{EM}}} = \frac{\left( \frac{\omega_p}{\omega} \right)^2 \int_a^d |\tilde{E}_z|^2 dy}{\int_0^d \{ \varepsilon_r(y) |\tilde{E}|^2 + c^2 |\tilde{B}_x|^2 \} dy}, \quad (6)$$



TABLE I. Values of parameters used in numerical simulation.

	I	II	III	Unit
<b>Waveguide</b>				
Dielectric thickness $a$	0.75	0.75	0.75	mm
Separation between two conducting plates $d$	3.0	3.0	3.0	mm
Relative permittivity $\epsilon_r$	2.12	2.12	2.12	
<b>Electron beam</b>				
Dielectric-beam gap $f-a$	0.4	0.4	0.4	mm
Beam thickness $g-f$	0.4	0.4	0.4	mm
	(0.8)	(0.8)	(0.8)	
Plasma frequency $\omega_p/2\pi$	477	477	477	MHz
Electron density $N_b$	4.92	4.85	4.32	$\times 10^9 \text{ cm}^{-3}$
Initial drift velocity $\beta_0$	0.819	0.813	0.757	
Initial beam voltage	380	367	271	kV
Initial beam current	0.77	0.76	0.63	A/cm
	(1.55)	(1.52)	(1.26)	
<b>Background plasma</b>				
Plasma frequency $\omega_p/2\pi$	140	—	—	GHz
Plasma density $N_p$	2.43	—	—	$\times 10^{14} \text{ cm}^{-3}$
<b>EM wave</b>				
Initial EM power	10	10	10	$\mu\text{W/cm}$
Operating frequency $\omega/2\pi$	129	89.4	129	GHz
Guide wavelength $\lambda_g$	1.89	2.72	1.76	mm

where

$$\epsilon_r(y) = \begin{cases} \epsilon_r & (0 < y < a) \\ 1 & (a < y < d). \end{cases}$$

Here,  $|\tilde{E}|$ ,  $|\tilde{E}_z|$  and  $|\tilde{B}_x|$  denote the absolute values of the Fourier amplitudes for the total electric field, the axial electric field and the transverse magnetic field, respectively.

To carry out a numerical calculation of the EM wave growth, the interaction region in our Cherenkov laser model is divided into a large number of small segments along the  $z$  direction, in each of which the beam drift velocity is assumed to be constant. On the basis of the fluid model of the electron beam, we numerically solve the dispersion relation described in the foregoing section for a spatial growth rate in each segment, and follow step by step the growth in the EM power according to the coupled-mode theory.<sup>18</sup> By using the principle of energy conservation, we eventually have<sup>19</sup>

$$\gamma_{n+1} = -\frac{\Delta P_n}{m_0 c^2 N V (g-f)} + \frac{1}{\sqrt{1-\beta_n^2}}, \quad (7)$$

$$\beta_{n+1} = \sqrt{1 - \frac{1}{\gamma_{n+1}^2}}$$

where,  $\Delta P_n$ ,  $N$ ,  $V$ ,  $\beta_n$  and  $\beta_{n+1}$  denote, respectively, the increment of the EM power in the  $n$ th segment, the average electron number density, the drift velocity of the electron beam, and the normalized drift velocities in the  $n$ th and  $(n+1)$ th segments.

The values of parameters used in the numerical simulation are listed in Table I. For the thin film technology which is available nowadays, the value of dielectric thickness  $a$  shown in Table I is considered reasonable. To compare the numerical results between the system with and without back-

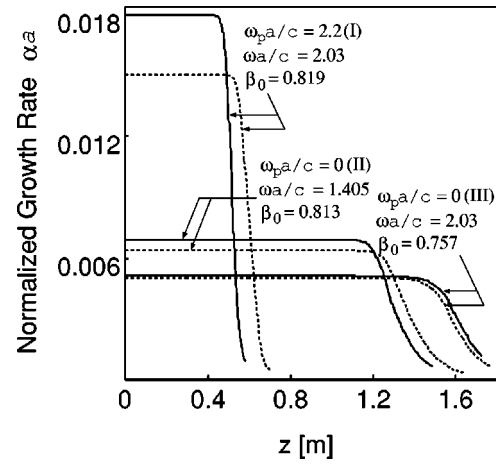


FIG. 5. Temporal variation of spatial growth rate. Solid and broken lines represent the results for the beam thickness of 0.8 and 0.4 mm.

ground plasma, we select points I and II in Fig. 1, which provide the maximum value of the spatial growth rate for each case. At the two points, the electron beams with slightly different values of the normalized beam velocity  $\beta$  equal to 0.819 and 0.813 are used, synchronizing with the EM waves at operating frequencies of 129 and 89.4 GHz, respectively. Point III in Fig. 1 is also picked out to compare with the plasma-filled device at the same operating frequency of 129 GHz, but at a lower beam velocity  $\beta=0.757$ . In all cases, two values of the beam thickness 0.4 and 0.8 mm are used. Beam currents corresponding to the beam thickness of 0.8 mm are shown in brackets in Table I. In the numerical calculation, the length of each segment in the  $z$  direction is determined in such a way that the relative variation of  $\beta$  between successive segments does not exceed 0.01%.

The numerical results in Fig. 5 illustrate how the spatial growth rate  $\alpha$  varies along the  $z$  direction. In every case, at the beginning of the process when the EM power level remains very low, the spatial growth rate varies only slightly, but decreases more and more rapidly as the EM wave gradually grows and gets out of synchronism with the electron beam. The spatial growth rate finally drops down to zero, when the EM wave stops growing and reaches saturation. As is evident from Fig. 5, the growth characteristics of the Cherenkov laser are greatly enhanced by the injection of background plasma. We observe that the system with background plasma reaches saturation earlier than that without background plasma. Hence, the size of a Cherenkov device with background plasma can become more compact by a more reasonable interaction length. When we use a thicker beam, the spatial growth rate in the plasma-filled device is significantly improved, while it is only slightly enhanced in that of the vacuum. This is because in the plasma-filled device, the longitudinal electric field distribution varies less steeply over the beam cross section, contributing to the enhancement of the beam-wave interaction.

Figure 6 shows the rate of energy transfer from the relativistic electron beam to the EM wave and the background plasma  $\eta$ , which can be calculated from the decrease in the beam energy as

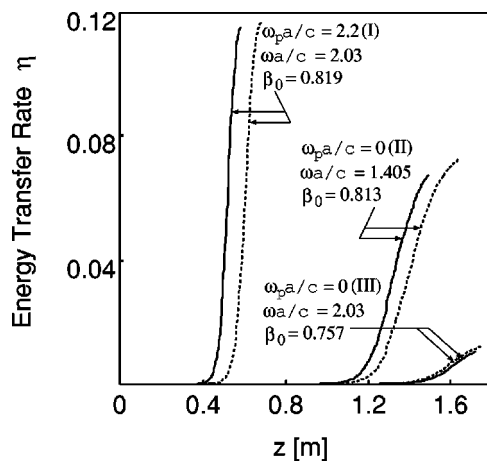


FIG. 6. Temporal variation of beam-wave energy transfer rate. Solid and broken lines represent the results for the beam thickness of 0.8 and 0.4 mm.

$$\eta = \frac{W_p^0 - W_p}{W_p^0}, \quad (8)$$

where  $W_p$  represents the kinetic energy of the electron beam at a certain time, and  $W_p^0$  is that at the initial state. As is evident from Fig. 6, the energy transfer rate in the system with the background plasma is greatly enhanced. Nevertheless, the growth in the kinetic energy of background plasma somewhat affects the EM energy level. With the values of parameters used in our numerical simulation, however, the ratio of the kinetic energy gained by the background plasma to the EM wave energy does not exceed 0.06 for the operating frequency at 129 GHz ( $\omega a/c = 2.03$ ).

#### IV. REMARKS AND CONCLUSION

With the aid of numerical simulations based upon the fluid model of the electron beam, the amplification characteristics of a 2-D plasma-filled Cherenkov laser in the millimeter wave region were discussed. We found that a Cherenkov laser with background plasma can generate a higher EM output power with a larger beam current, and can also operate at higher frequencies. An effective interaction of the relativistic electron beam with the EM wave within the plasma region provided an enhanced spatial growth rate for the EM wave. As a result, the Cherenkov laser with background plasma reached a saturation state more rapidly at a shorter interaction length, suggesting the possibility of a more compact device. Moreover, in order to gain more effective beam-wave coupling, it was possible to use a beam with larger thickness in a plasma-filled device.

In this paper, we also discussed the effect of electron-ion collision in the background plasma. The presence of the electron-ion collision results in a noticeable decrease in the spatial growth rate for the coupled waves. Nevertheless, by proper choices of the plasma and beam parameters, the value of the spatial growth rate was found to remain well over that for the vacuum device.

For simplicity, a sufficiently large static axial magnetic field was assumed to be applied to our model to restrict the movement of the background plasma and the electron beam only in one specific direction. In fact, an important role of the background plasma in neutralizing the space-charge force in the electron beam can help relax the requirements on beam focusing and alignment. Therefore, thanks to this beneficial feature of the background plasma, we can down-size the device by making use of smaller solenoids used for generating a guiding magnetic field.<sup>12</sup> Furthermore, in our analysis, the background plasma was assumed to have a homogeneous density profile. As we may see from some experiments (see Ref. 13 for example), the background plasma in the real situation usually has an inhomogeneous density profile. In our next work, we will discuss the effect of an inhomogeneous background plasma injected in the Cherenkov laser.

Finally, we wish to draw some conclusions regarding slow-wave structures. In this article we discussed the effect of background plasma injected into the Cherenkov laser, in which a dielectric waveguide is used for the slow-wave structure. However, similar results can also be expected for the Smith-Purcell free-electron laser, which uses the slow-wave structure composed of a metallic grating.

#### ACKNOWLEDGMENT

A part of this work was supported by a grant-in-aid for Scientific Research of the Ministry of Education, Science, Sports, and Culture of Japan.

- <sup>1</sup>J. E. Walsh, T. C. Marshall, and S. P. Schlessinger, *Phys. Fluids* **20**, 709 (1977).
- <sup>2</sup>K. L. Felch, K.O. Busby, R. W. Layman, D. Kapilow, and J. E. Walsh, *Appl. Phys. Lett.* **38**, 601 (1981).
- <sup>3</sup>J. E. Walsh, *Phys. Rev. Lett.* **66**, 699 (1991).
- <sup>4</sup>J. E. Walsh and J. B. Murphy, *IEEE J. Quantum Electron.* **QE-18**, 1259 (1982).
- <sup>5</sup>T. Shiozawa and H. Kondo, *IEEE J. Quantum Electron.* **QE-23**, 1644 (1987).
- <sup>6</sup>Y. Shibuya and T. Shiozawa, *IEICE Trans.* **E72**, 828 (1989).
- <sup>7</sup>T. Ueda and T. Shiozawa, *Appl. Phys. Lett.* **67**, 3838 (1995).
- <sup>8</sup>A. Hirata and T. Shiozawa, *IEEE J. Quantum Electron.* **QE-34**, 1802 (1998).
- <sup>9</sup>*Applications of High-Power Microwave* edited by A. V. Gaponov-Grekhov and V. L. Granatstein (Artech House, Norwood, MA, 1994).
- <sup>10</sup>Y. Carmel, K. Minami, R. A. Kehs, W. W. Destler, V. L. Granatstein, D. Abe, and W. L. Lou, *Phys. Rev. Lett.* **62**, 2389 (1989).
- <sup>11</sup>H. Kosai, E. P. Garate, and A. Fisher, *IEEE Trans. Plasma Sci.* **18**, 1002 (1990).
- <sup>12</sup>G. S. Nusinovich, Y. Carmel, T. M. Antonsen, D. M. Goebel, and J. Santoru, *IEEE Trans. Plasma Sci.* **26**, 628 (1998).
- <sup>13</sup>A. G. Shkvarunets, S. Kobayashi, Y. Carmel, J. Rodgers, T. M. Antonsen, Jr., L. Duan, and V. L. Granatstein, *IEEE Trans. Plasma Sci.* **26**, 646 (1998).
- <sup>14</sup>B. N. Brejzman and D. D. Rutov, *Nucl. Fusion* **14**, 879 (1974).
- <sup>15</sup>V. S. Burmasov, I. V. Kandaurov, E. P. Kruglyakov, and O. I. Meshkov, *IEEE Trans. Plasma Sci.* **23**, 952 (1995).
- <sup>16</sup>T. Shiozawa and T. Nakashima, *J. Appl. Phys.* **55**, 637 (1984).
- <sup>17</sup>V. L. Ginzburg, *Electromagnetic Waves in Plasmas* (Pergamon, New York, 1964).
- <sup>18</sup>W. H. Louisell, *Coupled Mode and Parametric Electronics* (Wiley, New York, 1960).
- <sup>19</sup>T. Shiozawa and H. Kamata, *IEEE J. Quantum Electron.* **QE-33**, 1687 (1997).